Letter   Editors' Suggestion

Highly Efficient Spin-Current Generation by the Spin Hall Effect in $Au_{1-x}Pt_x$

Lijun Zhu,[1,*] Daniel. C. Ralph,[1,2] and Robert A. Buhrman[1]

[1]*Cornell University, Ithaca, New York 14850, USA*
[2]*Kavli Institute at Cornell, Ithaca, New York 14853, USA*

We report very efficient spin-current generation by the spin Hall effect in the alloy $Au_{0.25}Pt_{0.75}$, which, as determined by two different direct spin-orbit torque measurements, exhibits a giant internal spin Hall ratio of ≥ 0.58 (antidamping spin-orbit torque efficiency of approximately 0.35 in bilayers with Co), a relatively low resistivity of approximately $83\,\mu\Omega$ cm, an exceptionally large spin Hall conductivity of $\geq 7.0 \times 10^5\,\Omega^{-1}\,m^{-1}$, and a spin diffusion length of 1.7 nm. This work establishes $Au_{0.25}Pt_{0.75}$ as a milestone spin-current generator that provides greater energy efficiency than that yet obtained with other heavy metals or with the topological insulators Bi_2Se_3 and $(Bi, Se)_2Te_3$. Our findings should advance spin-orbit torque-based fundamental research and benefit the development of fast, efficient spin-orbit torque-driven magnetic memories, skyrmion and chiral domain wall devices, and microwave and terahertz emitters.

I. INTRODUCTION

Current-induced spin-orbit torques (SOTs) in heavy metal/ferromagnet (HM/FM) systems have attracted considerable attention due to their potential for application in the efficient manipulation of magnetization at the nanoscale [1–6]. The pure transverse spin-current density j_s arising from an applied longitudinal electrical density j_e via the spin Hall effect (SHE) in HMs can generate dampinglike SOT sufficiently strong to excite magnetization dynamics at microwave or terahertz frequencies [3,4], create and move skyrmions [5], drive chiral domain wall displacement [6], or switch the magnetization of thin-film nanomagnets [1,2]. Of particular technological promise are the HMs with a large spin Hall ratio (θ_{SH}), or more precisely with a large dampinglike SOT efficiency $\xi_{DL} \equiv T_{int}\theta_{SH} \equiv T_{int}(2e/\hbar)j_s/j_e$, which is exerted on an adjacent ferromagnetic layer, as these could allow for the development of very fast, deterministic, and efficient magnetic random-access memories (MRAMs). Here, T_{int} (<1) is the spin transparency of the HM/FM interface. For example, the SHE in Pt (W) has been recently demonstrated to switch in-plane magnetic tunnel junctions with a critical switching current density of 4.0 (0.54) $\times 10^7$ A/cm² and a write error rate below 10^{-5} (10^{-6}) with a 2-ns pulse duration [7,8]. Despite extensive efforts, the efficiency of present SOT operations is still limited by a relatively low ξ_{DL} and/or a very high resistivity (ρ_{xx}) of the HM. For instance, β-W has a large $|\xi_{DL}|$ of approximately 0.3, but is very resistive

($\rho_{xx} \approx 300\,\mu\Omega$ cm at 4 nm) [9]; $|\xi_{DL}|$ generally reported for Pt and β-Ta is comparatively low (approximately -0.12), and β-Ta is also very resistive (almost equal to $180\,\mu\Omega$ cm) [1,10]. These factors lead to an undesirably large energy dissipation.

It has been established that the SHE in Pt is generally dominated by the intrinsic band structure effect [11,12] with the spin Hall conductivity $\sigma_{SH} \equiv \sigma_{SH}^{intr} + \sigma_{SH}^{extr} \approx \sigma_{SH}^{intr}$. Here, σ_{SH}^{intr} and σ_{SH}^{extr} are the intrinsic and extrinsic contributions. Hence, ξ_{DL} $[= T_{int}(2e/\hbar)\sigma_{SH}\rho_{xx}]$ can be enhanced by raising ρ_{xx} provided that σ_{SH} is not degraded in the process. Some success has been achieved in this manner by alloying Pt with Hf or with Al, but the maximum ξ_{DL} is still below 0.16 even when ρ_{xx} is enhanced to $110\,\mu\Omega$ cm, presumably due to a decrease in σ_{SH} with increasing Hf or Al concentration [10]. Recently theoretical work has suggested that alloying Pt with Au would be particularly effective in increasing ξ_{DL} via raising ρ_{xx}, due to a slower reduction in σ_{SH} at high Pt concentration [13]. Here, we report from direct SOT measurements that the $Au_{1-x}Pt_x$ alloy is indeed an enhanced spin-current generator, with a maximum ξ_{DL} of 0.35 while still maintaining a relatively low ρ_{xx} almost equal to $83\,\mu\Omega$ cm and a relatively long spin diffusion length (λ_s) of 1.7 nm for the optimized composition $x = 0.75$. We also determine a lower bound for θ_{SH} of 0.58 and a lower bound for the σ_{SH} of $7.0 \times 10^5\,\Omega^{-1}\,m^{-1}$ for $Au_{0.25}Pt_{0.75}$. While the variation of ξ_{DL} with Pt concentration x is qualitatively similar in form to the theoretical prediction, both θ_{SH} and σ_{SH} are much greater, approximately twice, than both the theoretical prediction and the experimental results from the indirect spin pumping/inverse SHE measurements reported in Ref. [13].

*lz442@cornell.edu

II. RESULTS AND DISCUSSIONS

A. Samples and characterizations

The samples for this work include two series of multilayer stacks: (I) Ta 1.0/$Au_{1-x}Pt_x$ 4.0/Co 0.8–1.4/MgO 2.0/Ta 1.5 (numbers are thicknesses in nm) with $x = 0$, 0.25, 0.5, 0.65, 0.75, 0.85, and 1, respectively; (II) Ta 1.0/$Au_{0.25}Pt_{0.75}$ 0, 2, 3, 4, 5, 6, and 8/Co 0.8–1.4/MgO 2.0/Ta 1.5 [Fig. 1(a)]. All the stacks are sputtered at room temperature on SiO_2/Si wafers with an argon pressure of 2 mTorr and a base pressure of below 1×10^{-8} Torr. The 1-nm Ta underlayer is introduced to improve the adhesion and uniformity of the $Au_{1-x}Pt_x$ layer, but is expected to contribute negligible spin current into the Co layer as a consequence of the small thickness and high ρ_{xx} of Ta, the short λ_s of $Au_{1-x}Pt_x$, and the opposite signs of ξ_{DL} for Ta and $Au_{1-x}Pt_x$. The 1.5-nm Ta capping layer is fully oxidized upon exposure to the atmosphere. X-ray diffraction studies show that, as is the case with the elemental metals Au and Pt, $Au_{1-x}Pt_x$ has a face-centered-cubic structure with the $Au_{1-x}Pt_x$ (111) peak shifting from Pt to Au with increasing Au concentration [Fig. 1(b)], indicating the variation of the lattice constant according to Vegard's Law [Fig. 1(c)]. Vibrating sample magnetometer measurements as a function of Co thicknesses (t) show that there is no significant magnetic dead layer at the $Au_{1-x}Pt_x$/Co and Co/MgO interfaces and that the Co layers have an almost x independent saturation magnetization (M_s) of 1413 ± 82 emu/cc [14], which is slightly smaller than the Co bulk value of approximately 1450 emu/cc and indicative of the absence of a significant magnetic proximity effect [15].

As shown in Fig. 1(d), the stacks are patterned into $5 \times 60 \ \mu m^2$ Hall bars by ultraviolet photolithography and argon ion milling. The $Au_{1-x}Pt_x$ resistivity for each composition (x) and thickness (d) is determined by measuring the conductance enhancement of the corresponding stacks ($d > 0$ nm) with respect to the $d = 0$ nm stack. The Co resistivity is determined to be approximately 80 and 65 $\mu\Omega$ cm for 0.85 and 1.4 nm thicknesses, respectively, higher than bulk Co due to the strong interfacial scattering. For harmonic response measurements, a lock-in amplifier is used to source a sinusoidal voltage ($V_{in} = 4$ V) onto the bar (length $L = 60 \ \mu m$) orientated along the x axis and to detect the in-phase first- and out-of-phase second-harmonic Hall voltages, $V_{1\omega}$ and $V_{2\omega}$. The direct current switching of magnetization is measured with a dc current sourced by a Yokogawa 7651 and with the differential Hall resistance detected by the lock-in amplifier ($V_{in} = 0.1$ V).

B. Composition dependence of spin-orbit torques

Figure 1(e) shows three examples of the anomalous Hall voltage hysteresis loops of $Au_{1-x}Pt_x$ 4-nm/Co 0.8-nm bilayers with $x = 1$, 0.75, and 0.25, where the fairly square loops and large H_c provide evidence of the strong perpendicular magnetic anisotropy (PMA) of these samples. All the samples with $x \geq 25\%$ exhibit good PMA, H_c larger than 500 Oe, and perpendicular anisotropy field H_k of 6–12 [14]. The strong PMA allows us to obtain high-quality out-of-plane harmonic response data. Pure Au/Co bilayers do not show PMA in the studied Co thickness range. We carry out in-plane harmonic response measurements on $Au_{1-x}Pt_x$ 4/Co 1.4 bilayers with in-plane magnetic
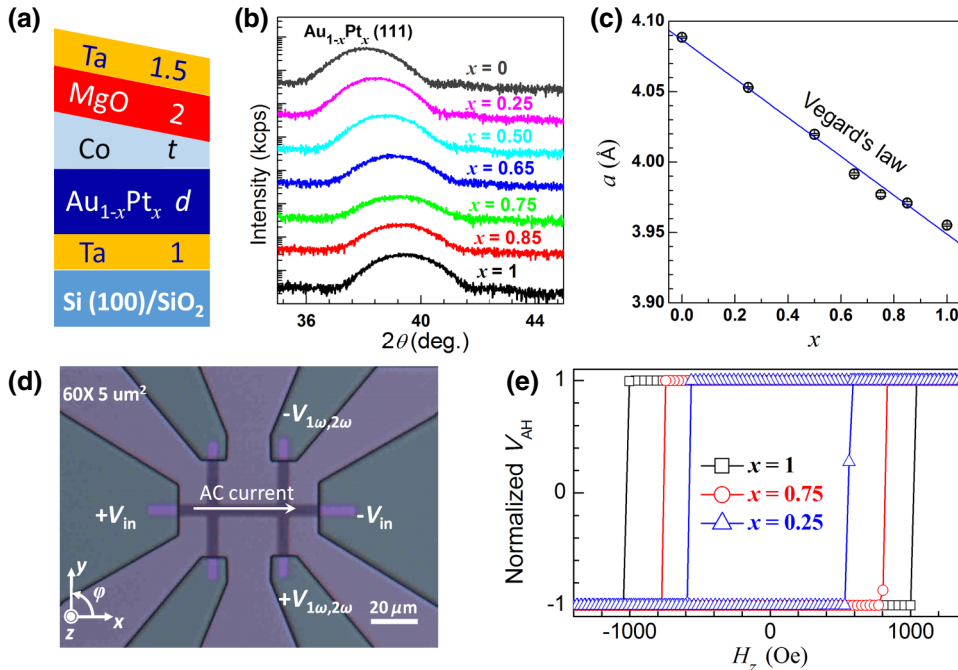

FIG. 1. (a) Schematic depiction of the magnetic stacks with t and d being the thicknesses of Co and $Au_{1-x}Pt_x$ layers in nm. (b) X-ray diffraction patterns for different $Au_{1-x}Pt_x$ composition x. (c) Lattice constant of $Au_{1-x}Pt_x$ plotted as a function of x. (d) Optical microscopy image of a Hall bar device showing the geometry and the measurement coordinate. (e) Normalized anomalous Hall voltage for $Au_{1-x}Pt_x$ 4/Co 0.8 bilayers ($x = 1$, 0.75, and 0.5, respectively).
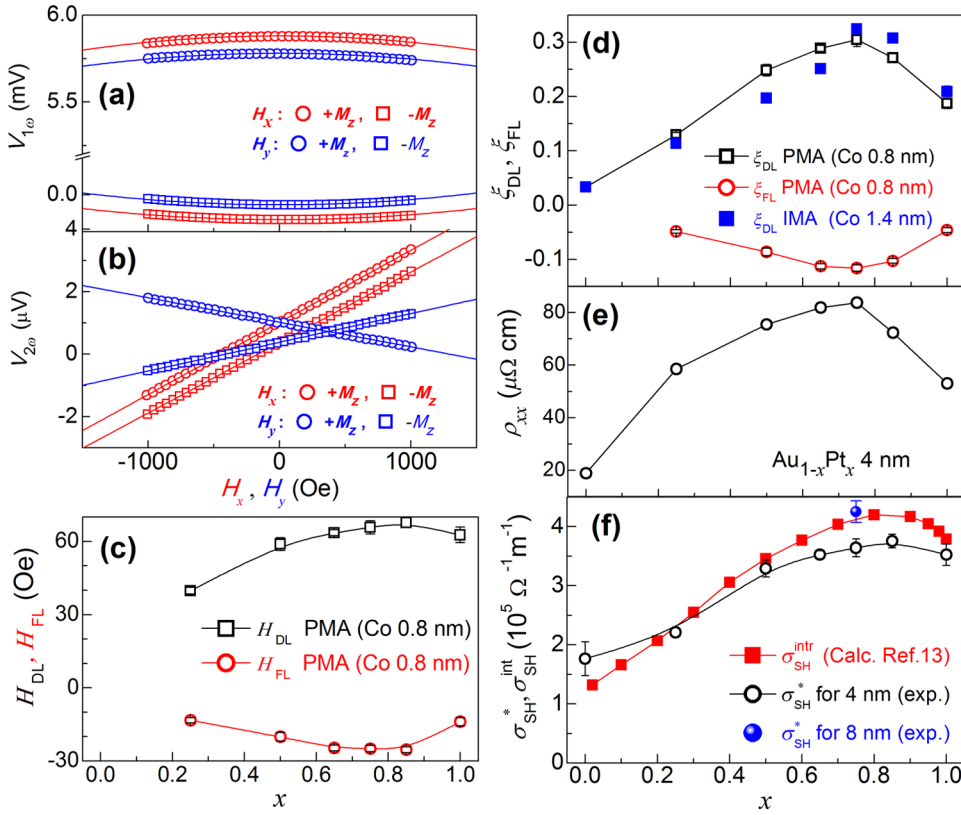
FIG. 2. (a) The first ($V_{1\omega}$) and (b) second ($V_{2\omega}$) harmonic voltages plotted as a function of in-plane fields H_x (red) and H_y (blue), respectively (for $x = 0.75$); Composition dependence of (c) effective spin-torque fields H_{DL} and H_{FL}, (d) spin-torque efficiencies ξ_{DL} and ξ_{FL}, (e) Au$_{1-x}$Pt$_x$ resistivity ρ_{xx}, and (f) *calculated* intrinsic spin Hall conductivity σ_{SH}^{intr} for bulk Au$_{1-x}$Pt$_x$ (red squares) and experimentally measured effective spin Hall conductivity $\sigma_{SH}^* \equiv T_{int}\sigma_{SH}$, where $T_{int} \cong 0.6$ if there is no spin memory loss at the Au$_{1-x}$Pt$_x$/Co interfaces, for 4-nm (black circle) and 8-nm Au$_{0.25}$Pt$_{0.75}$ (blue solid dot), respectively. For clarity, the H_y-dependent $V_{1\omega}$ data (the blue points) in (a) are artificially shifted by ± 0.001 mV for $\mp M_z$, respectively.

anisotropy (IMA) to reaffirm the SOT efficiencies for each x from 0 to 1.

We first discuss the SOTs in 4-nm Au$_{1-x}$Pt$_x$ samples with different x. Figures 2(a) and 2(b) shows an example of $V_{1\omega}$ and $V_{2\omega}$ to an applied ac current for perpendicularly magnetized Au$_{1-x}$Pt$_x$ 4/Co 0.8 bilayers ($x \geq 0.25$) as a function of in-plane bias fields H_x and H_y, from which the dampinglike and fieldlike effective spin-torque fields are determined by $H_{DL(FL)} = -2(\partial V_{2\omega}/\partial H_{x(y)})/(\partial^2 V_{1\omega}/\partial^2 H_{x(y)})$. As summarized in Fig. 2(c), both H_{DL} and H_{FL} are significantly tuned by x. Figure 2(d) shows ξ_{DL} and fieldlike SOT efficiency ξ_{FL} calculated by $\xi_{DL(FL)} = 2e\mu_0 M_s tH_{DL(FL)}/\hbar j_e$, with e, μ_0, t, $\hbar$, and $j_e = V_{in}/L\rho_{xx}$ being the elementary charge, the permeability of vacuum, the ferromagnetic layer thickness, the reduced Planck constant, and the charge current density, respectively. Most notably, ξ_{DL} climbs up quickly from 0.03 at $x = 0$ (pure Au) to the peak value of 0.30 at $x = 0.75$ and then gradually drops to 0.18 at $x = 1$ (pure Pt). We consistently observe the same x dependence with in-plane harmonic measurements [14] of ξ_{DL} on Au$_{1-x}$Pt$_x$ 4/Co 1.4 IMA samples [Fig. 2(d)]. We note here that a ξ_{DL} of 0.18 for the 4 nm pure Pt sample is larger than 0.12 as previously reported for Pt/Co bilayers [16], but in that case, ρ_{xx} was 28 $\mu\Omega$ cm due to specific details of the thin-film growth process. The giant ξ_{DL} of 0.30 for the 4-nm Au$_{0.25}$Pt$_{0.75}$ is comparable to the high value reported for

β-W [9] and three times higher than that of β-Ta [1]. One of the important factors that determines the nonmonotonic x dependence is the variation in ρ_{xx} of the alloys. As can be clearly seen in Fig. 2(e), ρ_{xx} of 4-nm Au$_{1-x}$Pt$_x$ thin film varies significantly and peaks at $x = 0.75$ due to enhanced electron scattering at that alloy concentration. We note that the maximum ρ_{xx} is 83 $\mu\Omega$ cm for Au$_{0.25}$Pt$_{0.75}$, approximately one fourth that of β-W [9], which represents a considerable improvement of energy efficiency for SOT applications. ξ_{FL} is negative and small in magnitude relative to ξ_{DL}, and scales with ξ_{DL}, consistent with the SHE in Au$_{1-x}$Pt$_x$ alloys being the dominant source of both spin torques.

In Fig. 2(f), we plot the apparent spin Hall conductivity $\sigma_{SH}^* \equiv T_{int}\sigma_{SH} = (2e/\hbar)\mu_0 M_s tH_{DL}\rho_{xx}/j_e$ as a function of x using the experimental results shown in Figs. 2(c) and 2(e). Assuming that T_{int} is approximately independent of x in the high Pt-concentration regime, this plot indicates that σ_{SH} remains constant or even initially increases slightly for decreasing x in the Pt-rich regime, $0.6 < x \leq 1.0$. Moreover, as is also shown in Fig. 2(f), the measured σ_{SH}^* for the 4-nm samples has a functional x dependence similar to a recent calculation of σ_{SH}^{intr} for bulk Au$_{1-x}$Pt$_x$ [13], which supports the conclusion that in this system the intrinsic spin Hall contribution arising from the topology of the electronic band structure is dominant.
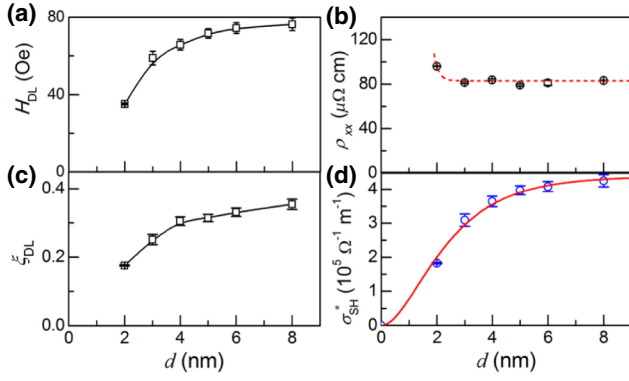
FIG. 3. $Au_{0.25}Pt_{0.75}$ thickness dependences of (a) H_{DL}, (b) ξ_{DL}, (c) ρ_{xx}, and (d) σ_{SH}^*, respectively.

C. Spin diffusion length and spin Hall conductivity

The spin diffusion length is a key parameter for the theoretical understanding of a spin Hall material, for determining θ_{SH} via inverse SHE experiments, and for optimizing SOT effectiveness. We determine λ_s for $Au_{0.25}Pt_{0.75}$ by out-of-plane harmonic measurements of H_{DL} and ξ_{DL} for a series of $Au_{0.25}Pt_{0.75}$ d/Co 0.8 bilayers as a function of thickness d. The results plotted in Figs. 3(a) and 3(b) show that H_{DL} and ξ_{DL} increase as d increases, as expected from the "bulk" SHE, with ξ_{DL} saturating at approximately 0.35 by $d = 8$ nm. In Fig. 3(c), we plot the resistivity of the $Au_{0.25}Pt_{0.75}$ layers as a function of d showing that ρ_{xx} reaches its bulk value of 83 $\mu\Omega$ cm by $d \approx 3$ nm, consistent with a high-resistivity material

having a short bulk mean free path. In Fig. 3(d), we p lot σ_{SH}^* of the $Au_{0.25}Pt_{0.75}$ alloy. If we assume that the SOT arises entirely from the SHE of $Au_{0.25}Pt_{0.75}$ as indicated by the d dependence of ξ_{DL} and that the interfacial spin mixing conductance $G^{\uparrow\downarrow} \approx \text{Re}G^{\uparrow\downarrow} \gg \text{Im}G^{\uparrow\downarrow}$, we can obtain λ_s and σ_{SH} following $\sigma_{SH}^* = \sigma_{SH}[1 - \text{sech}(d/\lambda_s)]$ $(1 + \tanh(d/\lambda_s)/2\lambda_s\rho_{xx}\text{Re}G^{\updownarrow})^{-1}$ [17]. This assumes that T_{int} is set by the spin backflow of an ideal $Au_{0.25}Pt_{0.75}$/Co interface with no interfacial spin-flip scattering (spin memory loss). We use $\rho_{xx} = 83\,\mu\Omega$ cm and, as an approximation, $G^{\uparrow\downarrow} \approx 5.9 \times 10^{14}\,\Omega^{-1}\text{m}^{-2}$, as calculated for the Pt/Co interface [17] to fit the data as shown by the solid line in Fig. 3(d). This fit ignores the slight variation in ρ_{xx} for small d and any change in λ_s with that variation. From this fit we determine $\lambda_s \approx 1.7 \pm 0.1$ nm, $\sigma_{SH} \approx (7.0 \pm 0.1) \times 10^5\,\Omega^{-1}\,\text{m}^{-1}$, and an internal spin Hall ratio $\theta_{SH} = 0.58 \pm 0.01$. This value for λ_s together with the measured ρ_{xx} corresponds to a $Au_{0.25}Pt_{0.75}$ spin conductance $1/\lambda_s\rho_{xx} \approx 0.71 \times 10^{15}\,\Omega^{-1}\,\text{m}^{-2}$, approximately 40% less than $1.25 \times 10^{15}\,\Omega^{-1}\,\text{m}^{-2}$ obtained for pure Pt from a similar thickness-dependent study [12]. Given the large value for σ_{SH} obtained from this thickness-dependent measurement, which, as it assumes an ideal $Au_{1-x}Pt_x$/Co interface, is perhaps just a lower bound, the proximity of the measured σ_{SH}^* value for $d \approx 8$ nm to the theoretically calculated value [13] also shown in Fig. 2(d) is fortuitous. Instead our measurements are indicating that internal σ_{SH} for $Au_{0.25}Pt_{0.75}$ is much larger than yet calculated, in accord with the results previously found for pure Pt [12]. Finally, we note that the value for λ_s here is considerably larger than the approximately 0.2 nm (less than one atomic
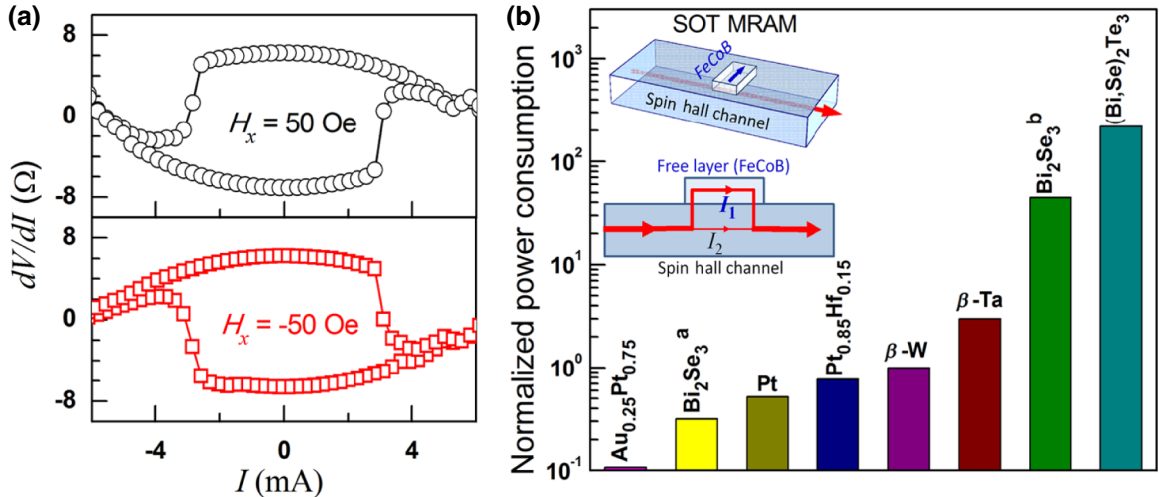

FIG. 4. (a) Deterministic direct current switching of a 0.8-nm perpendicularly magnetized Co layer with coercivity of 800 Oe and perpendicular anisotropy field of 6620 Oe via the dampinglike SOT generated by the giant SHE of a 4-nm $Au_{0.25}Pt_{0.75}$ layer. Magnetic fields of ± 50 Oe are applied along the current direction, respectively. (b) Normalized power consumption as calculated for a typical SOT-MRAM device with the different spin Hall channel materials listed in Table I. Insets: schematics of a SOT-MRAM device and its side view highlighting the increase of the write current due to the current shunting into the magnetic free layer.

TABLE I. Comparison of ξ_{DL}, ρ_{xx}, and σ_{SH}^* of various spin Hall materials.

	ξ_{DL}	ρ_{xx} $(\mu\Omega\,cm)$	σ_{SH}^* $(10^5\,\Omega^{-1}\,m^{-1})$	Ref.
β-Ta	0.12	190	0.63	[1]
β-W	0.3	300	1.0	[9]
Pt	0.12	50	2.4	[12]
$Pt_{0.85}Hf_{0.15}$	0.16	110	1.5	[10]
Bi_2Se_3[a]	3.5	1755	2.0	[19]
Bi_2Se_3[b]	0.16	1060	0.15	[20]
$(Bi, Se)_2Te_3$	0.4	4020	0.1	[20]
$Au_{0.25}Pt_{0.75}$	0.35	80	4.4	This work

layer) used in the extraction of θ_{SH} in $Au_{1-x}Pt_x/Ni_{81}Fe_{19}$ bilayers from spin pumping and inverse SHE measurements [13]. This latter technique also requires a quite accurate determination of $G^{\uparrow\downarrow}$, which can be challenging to achieve, particularly if there is significant spin memory loss at the interface [16,18].

D. Energy efficiency for spin-torque applications

Finally, we point out that $Au_{0.25}Pt_{0.75}$ is a particularly notable spin Hall material for SOT research and technological applications. As an example, we first show in Fig. 4(a) the deterministic switching of a 0.8-nm-thick perpendicularly magnetized Co layer with a large PMA ($H_k \approx 6620$ Oe) and a high coercivity ($H_c \approx 800$ Oe) enabled by the giant ξ_{DL} generated by the SHE of $Au_{0.25}Pt_{0.75}$. The switching current of approximately 3 mA corresponds to $j_e = 1.2 \times 10^7$ A/cm² in the $Au_{0.25}Pt_{0.75}$ layer. A small magnetic field of ± 50 Oe is applied along the current direction to overcome the Dzyaloshinshii-Moriya interaction at the $Au_{0.25}Pt_{0.75}/Co$ interface. For technological applications, e.g., MRAMs, very efficient SOT switching of a FeCoB thin layer is of great interest. Figure 4(b) compares the write energy efficiency for SOT-MRAM applications based on various strong spin Hall channel materials whose ξ_{DL}, ρ_{xx}, and σ_{SH}^* are listed in Table I. Here, we calculate a MRAM device with a $400 \times 200 \times 4$ nm³ spin Hall channel and a $110 \times 30 \times 1.8$ nm³ FeCoB free layer (resistivity $\rho_{FeCoB} = 130\,\mu\Omega$ cm) by taking into account the current shunting into the free layer and by using the parallel-resistor model [see the inset of Fig. 4(b)] [14]. The write power consumption for $Au_{0.25}Pt_{0.75}$ is 5, 8, 10, and 30 times smaller than that for Pt, $Pt_{0.85}Hf_{0.15}$, β-W, and β-Ta, respectively. The SOT MRAMs based on topological insulators Bi_2Se_3 and $(Bi, Se)_2Te_3$, which are reported to have ξ_{DL} of 0.16–3.5 [19,20], also have much higher power consumption than $Au_{0.25}Pt_{0.75}$ due to the considerable current-shunting effect that is a consequence of their giant resistivity [e.g., $4020\,\mu\Omega$ cm for $(Bi, Se)_2Te_3$]. We also note that $Au_{0.25}Pt_{0.75}$ is compatible with sputtering techniques and the use of Si substrates which are preferable for integration technology, whereas Bi_2Se_3 and $(Bi, Se)_2Te_3$ require costly molecular beam epitaxy growth and GaAs or sapphire substrates [19,20]. The high ρ_{xx} of β-W, β-Ta, Bi_2Se_3, or $(Bi, Se)_2Te_3$ is also problematic for applications that require energy efficiency, e.g., the prospective implementation of SOT devices in cryogenic computing systems [21]. For example, use of a spin Hall material with a large resistivity will result in a high write impedance that is difficult for superconducting circuits in a cryogenic computing system to accommodate. Therefore, the combination of the giant ξ_{DL}, the relatively low resistivity, and the compatibility with sputtering and silicon integration technology makes $Au_{0.25}Pt_{0.75}$ a milestone spin Hall material for SOT research and technological applications.

III. CONCLUSIONS

We find $Au_{0.25}Pt_{0.75}$ to be a strong spin Hall material with a giant θ_{SH} of >0.58 (ξ_{DL} of 0.35 in bilayers with Co), a relatively low resistivity of $\sim 83\,\mu\Omega$ cm, a large σ_{SH} of $>7.0 \times 10^5\,\Omega^{-1}\,m^{-1}$, and λ_s of approximately 1.7 nm (assuming $G^{\uparrow\downarrow} \approx 5.9 \times 10^{14}\Omega^{-1}m^{-2}$). The giant θ_{SH} and ξ_{DL} arising from the intrinsic contribution of the SHE in $Au_{1-x}Pt_x$ alloys and the low resistivity make $Au_{0.25}Pt_{0.75}$ more energy efficient than all the other conventional HMs and the topological insulators Bi_2Se_3 and $(Bi, Se)_2Te_3$ whose spin Hall properties have yet to be reported. Our direct demonstration of the SOT efficiency of this milestone spin Hall material $Au_{0.25}Pt_{0.75}$ which simultaneously combines a giant charge-spin conversion efficiency, low resistivity, and chemical stability with excellent processing compatibility for device integration, paves the way for further fundamental research that will benefit from the efficient generation of spin currents and of spin-orbit torques, and for the development of highly efficient SOT-driven magnetic memories, skyrmion and chiral domain wall devices, and microwave and terahertz emitters.

[1] L. Liu, C.-F. Pai, Y. Li, H. W. Tseng, D. C. Ralph, and R. A. Buhrman, Spin-torque switching with the giant Spin hall effect of tantalum, Science **336,** 555 (2012).

[2] G. Yu, P. Upadhyaya, Y. Fan, J. G. Alzate, W. Jiang, K. L. Wong, S. Takei, S. A. Bender, L.-T. Chang, Y. Jiang, M. Lang, J. Tang, Y. Wang, Y. Tserkovnyak, P. K. Amiri, and K. L. Wang, Switching of perpendicular magnetization by spin–orbit torques in the absence of external magnetic fields, Nat. Nanotechnol. **9,** 548 (2014).

[3] V. E. Demidov, S. Urazhdin, H. Ulrichs, V. Tiberkevich, A. Slavin, D. Baither, G. Schmitz, and S. O. Demokritov, Magnetic nano-oscillator driven by pure spin current, Nat. Mater. **11,** 1028 (2012).

[4] Y. Wu, M. Elyasi, X. Qiu, M. Chen, Y. Liu, L. Ke, and H. Yang, High-performance THz emitters based on ferromagnetic/ nonmagnetic heterostructures, Adv. Mater. **29,** 1603031 (2017).

[5] W. Jiang, P. Upadhyaya, W. Zhang, G. Yu, M. B. Jungfleisch, F. Y. Fradin, J. E. Pearson, Y. Tserkovnyak, K. L. Wang, O. Heinonen, S. G. E. Velthuis, and A. Hoffmann, Blowing magnetic skyrmion bubbles, Science **349,** 283 (2015).

[6] P. P. J. Haazen, E. Muré, J. H. Franken, R. Lavrijsen, H. J. M. Swagten, and B. Koopmans, Domain wall depinning governed by the spin Hall effect, Nat. Mater. **12,** 299 (2013).

[7] S. V. Aradhya, G. E. Rowlands, J. Oh, D. C. Ralph, and R. A. Buhrman, Nanosecond-timescale low energy switching of in-plane magnetic tunnel junctions through dynamic Oersted-field-assisted spin Hall effect, Nano Lett. **16,** 5987 (2016).

[8] S. Shi, Y. Ou, S. V. Aradhya, D. C. Ralph, and R. A. Buhrman, Fast, Low-Current Spin-Orbit Torque Switching of Magnetic Tunnel Junctions Through Atomic Modifications of the Free Layer Interfaces, Phys. Rev. Applied **9,** 011002 (2018).

[9] C.-F. Pai, L. Liu, Y. Li, H. W. Tseng, D. C. Ralph, and R. A. Buhrman, Spin transfer torque devices utilizing the giant spin Hall effect of tungsten, Appl. Phys. Lett. **101,** 122404 (2012).

[10] M.-H. Nguyen, M. Zhao, D. C. Ralph, and R. A. Buhrman, Enhanced spin Hall torque efficiency in $Pt_{100-x}Al_x$ and $Pt_{100-x}Hf_x$ alloys arising from the intrinsic spin Hall effect, Appl. Phys. Lett. **108,** 242407 (2016).

[11] E. Sagasta, Y. Omori, M. Isasa, M. Gradhand, L. E. Hueso, Y. Niimi, Y. Otani, and F. Casanova, Tuning the spin Hall effect of Pt from the moderately dirty to the superclean regime, Phys. Rev. B **94,** 060412(R) (2016).

[12] M.-H. Nguyen, D. C. Ralph, and R. A. Buhrman, Spin Torque Study of the Spin Hall Conductivity and Spin Diffusion Length in Platinum Thin Films with Varying Resistivity, Phys. Rev. Lett. **116,** 126601 (2016).

[13] M. Obstbaum, M. Decker, A. K. Greitner, M. Haertinger, T. N. G. Meier, M. Kronseder, K. Chadova, S. Wimmer, D. Ködderitzsch, H. Ebert, and C. H. Back, Tuning Spin Hall Angles by Alloying, Phys. Rev. Lett. **117,** 167204 (2016).

[14] See supplementary materials at https://link.aps.org/supplemental/10.1103/PhysRevApplied.10.031001 for more details on the determination of saturation magnetization, perpendicular magnetic anisotropy, in-plane harmonics response measurements, and power consumption.

[15] C. L. Canedy, X. W. Li, and G. Xiao, Large magnetic moment enhancement and extraordinary Hall effect in Co/Pt superlattices, Phys. Rev. B **62,** 508 (2000).

[16] C.-F. Pai, Y. Ou, L. H. Vilela-Leao, D. C. Ralph, and R. A. Buhrman, Dependence of the efficiency of spin Hall torque on the transparency of Pt/ferromagnetic layer interfaces, Phys. Rev. B **92,** 064426 (2015).

[17] P. M. Haney, H.-W. Lee, K.-J. Lee, A. Manchon, and M. D. Stiles, Current induced torques and interfacial spin-orbit coupling: Semiclassical modeling, Phys. Rev. B **87,** 174411 (2013).

[18] J.-C. Rojas-Sánchez, N. Reyren, P. Laczkowski, W. Savero, J.-P. Attané, C. Deranlot, M. Jamet, J.-M. George, L. Vila, and H. Jaffrès, Spin Pumping and Inverse Spin Hall Effect in Platinum: The Essential Role of Spin-Memory Loss at Metallic Interfaces, Phys. Rev. Lett. **112,** 106602 (2014).

[19] A. R. Mellnik, J. S. Lee, A. Richardella, J. L. Grab, P. J. Mintun, M. H. Fischer, A. Vaezi, A. Manchon, E.-A. Kim, N. Samarth, and D. C. Ralph, Spin-transfer torque generated by a topological insulator, Nature **511,** 449 (2014).

[20] J. Han, A. Richardella, S. A. Siddiqui, J. Finley, N. Samarth, and L. Liu, Room-Temperature Spin-Orbit Torque Switching Induced by a Topological Insulator, Phys. Rev. Lett. **119,** 077702 (2017).

[21] D. S. Holmes, A. L. Ripple, and M. A. Manheimer, Energy-Efficient superconducting computing—power budgets and requirements, IEEE Trans. Appl. Supercond. **23,** 1701610 (2013).